COMPUTATIONAL FLUID DYNAMICS SIMULATION AND VALIDATION OF H₂S REMOVAL FROM FAN-VENTILATED CONFINED-SPACE MANURE STORAGES

J. Zhao, H. B. Manbeck, D. J. Murphy

ABSTRACT. *Confined-space manure storage entry is a major safety concern in the agricultural industry. An oxygen-deficient atmosphere as well as toxic and/or explosive gases (i.e., NH₃, H₂S, CH₄, and CO₂) often results from fermentation of the stored manure and accumulation in confined areas. These gases may create very hazardous conditions for farm workers who may need to enter these confined-space manure storages to work or perform maintenance. Hydrogen sulfide (H₂S) was used as an indicator gas to investigate the effectiveness of forced-ventilation strategies for eliminating the toxic and oxygen-deficient atmospheres in confined-space manure storages. The overall goal of this research was to develop and validate computational fluid dynamics (CFD) modeling protocols to simulate H₂S removal from fan-ventilated confined-space manure storages. The CFD model was used to identify the time taken to reach the OSHA permissible exposure limit of H₂S (T_{pel}). This article presents the CFD model simulations of evacuating H₂S during forced ventilation for the best ventilation strategies identified in previous research for a typical rectangular on-farm manure tank with three cover types (i.e., solid, fully slotted, and partially slotted) and the validation of the CFD modeling protocols based on comparisons between simulated and measured H₂S evacuation times. Simulated and measured evacuation times within the confined-space manure storages evaluated agreed within 10% at all measuring locations except those immediately adjacent to the ventilation fan jet for all three cover types for both high (5 AC min⁻¹) and low (3 AC min⁻¹) air exchange (AC) rates. Corresponding evacuation times agreed within 15% for all cover types and air exchange rates in the high-velocity gradient region of the ventilation fan jet.*

Keywords. *Computational fluid dynamics modeling protocols, Confined-space manure storages, Hydrogen sulfide, OSHA permissible exposure limit, Validation, Ventilation.*

The Occupational Safety and Health Administration (OSHA, 1998) definition of a confined space is one which "(1) is large enough and so configured that an employee can bodily enter and perform assigned work; (2) has limited or restricted means for entry or exit; and (3) is not designed for continuous employee occupancy." In the agricultural industry, below-ground manure storages are confined spaces, and entry into these confined spaces has been identified as a major safety concern. In confined-space manure storages, oxygen-deficient atmospheres as well as toxic and/or explosive gases resulting from fermentation of the stored manure create very hazardous conditions for farmers who may need to enter these storages to work or perform maintenance. The typical gases emitted from the manure include methane (CH_4), ammonia (NH_3), carbon dioxide (CO_2), and hydrogen sulfide (H_2S). Hydrogen sulfide is the primary toxic gas and may result in fatalities within minutes of exposure (Millar, 1990). This research focuses primarily on hydrogen sulfide. Hydrogen sulfide was used as an indicator gas to measure the effectiveness of candidate ventilation strategies for eliminating the toxic and oxygen-deficient atmospheres in confined-space manure storages. In addition, computational fluid dynamics (CFD) modeling protocols were validated using H_2S as an indicator gas for predicting the effectiveness of ventilation strategies for removing noxious gases from confined-space manure storages (Zhao, 2006; Pesce et al., 2007)

The health and safety issues associated with confined-space manure storages are well documented (e.g., CDC, 1993; Millar, 1990). Fatalities associated with on-farm confined-space manure storage facilities frequently occur when a victim enters an unventilated manure storage facility to make repairs or perform maintenance without wearing necessary personal protective equipment (PPE). Tragically, the accidents occurring in confined-space manure storages often involve multiple fatalities (Murphy and Steel, 2001). The accidents develop into multiple fatalities when other untrained and poorly equipped farm personnel attempt a rescue and become victims as well. Beaver and Field (2006) summarized documented fatalities in livestock manure storages and handling fatalities from 1975 to 2004. One result from this analysis of 77 fatality cases showed an increasing trend in the death rate per year between 1975 and 2004: 1.6 from 1975-1984, 2.7 from 1985-1994, and 3.5 from 1995-2004.

OSHA has developed confined-space regulations documented in the 29 Code of Federal Regulations (CFR) Part

1910.146. These regulations (summarized in OSHA, 2002) require that the internal atmosphere within a confined space be tested for oxygen levels, flammable gases and vapors, and potential noxious contaminants prior to human entry. According to OSHA standards, an employee may not enter a confined space until forced-air ventilation has eliminated any existing hazardous atmosphere. Thus, it is imperative that confined spaces be properly ventilated prior to entry. However, research studies on safety ventilation in confined-space manure storages are limited. Lloyd (2000) studied ventilation of a manure storage facility adjacent to a swine housing facility. In his research, airflow entry location and storage cover type could not be adjusted. These limitations in Lloyd's research were overcome by Pesce et al. (2007), who used a rectangular confined-space manure tank to identify the best ventilation strategies for each of three cover types: solid, fully slotted, and partially slotted. Alternative fan locations, cover types, and airflow rates were considered in Pesce's study. Figure 1 shows the best ventilation strategies identified from Pesce's research for three cover types at two air exchange (AC) rates (high: 5 AC min^{-1}, low: 3 AC min^{-1}). For the fully slotted and partially slotted cover types, the cover slots served as the outlet for the ventilation system. For the fully slotted and solid cover types, the identified best fan location was the same for the high and low air exchange rate (i.e., fan location in figs. 1a and 1b). The best ventilation strategies identified for the partially slotted cover type at the high and low air exchange rates had different fan locations (figs. 1c and 1d).

Computational fluid dynamics (CFD) modeling has been a useful tool for predicting air movement in ventilated spaces, including spatial variations in temperatures and pollutant concentrations (Sørensen and Nielsen, 2003). In this research, a CFD model was used to simulate H_2S concentration decrease during forced ventilation for the best ventilation strategies identified by Pesce et al. (2007). The time taken to reach the OSHA permissible exposure limit for H_2S (T_{pel}) (OSHA, 1995), the time taken to reach 50% of the initial gas concentration (gas concentration at the beginning of the ventilation) (T_{50}), the time taken to reach 25% of the initial concentration (T_{25}), and the time taken to reach 10% of the initial concentration (T_{10}) were identified from the CFD simulations performed. The H_2S emission rates and intercontamination ratios obtained experimentally (Zhao et al., 2007) were important input parameters for the CFD simulations. The CFD modeling protocols were validated based on the comparisons between simulated and measured time values (i.e., T_{pel}, T_{50}, T_{25}, and T_{10}). An extended validation of the CFD modeling protocols was performed using another independent manure storage facility. This manure storage facility was an underground manure reception pit adjacent to a mono-sloped naturally ventilated swine growing and finishing barn at the Pennsylvania State University Swine Research Center. The manure reception pit, which is a 3.04 × 3.04 × 3.04 m prismatic facility with a solid cover except for the pumping and agitation port and a closable manhole (also used to locate ventilation fan intake), is shown in figure 2.

CFD CODE AND TURBULENCE MODEL

In this research, PHOENICS (Parabolic, Hyperbolic, or Elliptic Numerical Integration Code Series, Version 3.6; CHAM, 2005) was the commercial CFD code used to perform simulations. As a generally applied CFD method for performing engineering simulations, Reynolds-average Navier-Stokes (RANS) solves Navier-Stokes governing equations using turbulence models (Versteeg and Malalasekera, 1995; Sun et al., 2007). Among the k–ε model and its variants, the standard k–ε turbulence model has been widely used to simulate indoor airflow under natural and mechanical ventilation in agricultural buildings (i.e., greenhouses, animal buildings) and residential buildings (Lee and Short, 2000; Holmberg and Chen, 2003). The standard k–ε turbulence model was used to perform simulations in this research because it yields stable results and is sufficient to perform general-purpose flow computations (Chen, 1995).

(a) Fully–slotted cover (high and low AC rates)

(b) Solid cover (high and low AC rates)

(c) Partially–slotted cover (high AC rate)

(d) Partially–slotted cover (low AC rate)
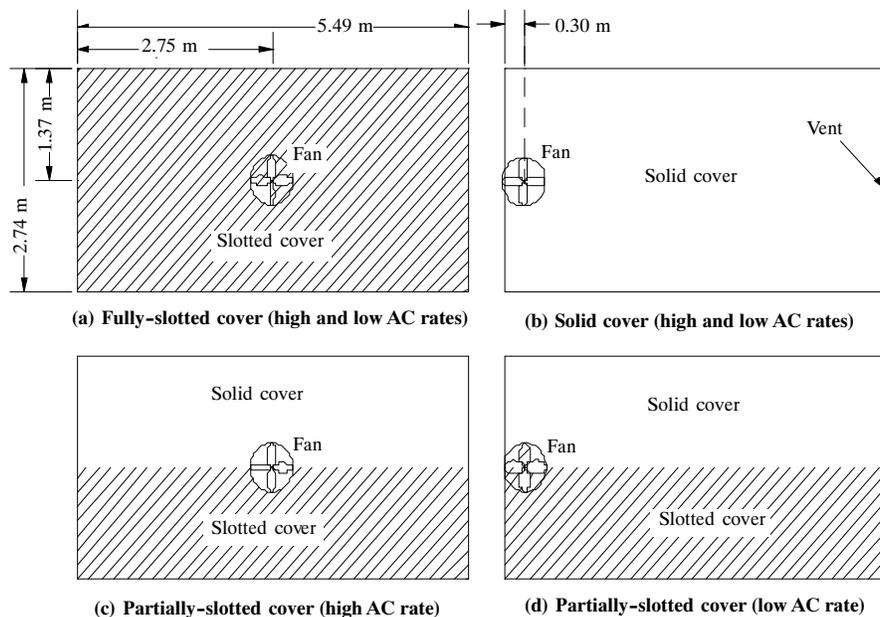
Figure 1. The best ventilation configurations for (a) fully slotted cover (high and low air exchange AC rates), (b) solid cover (high and low AC rates), (c) partially slotted cover (high AC rate), and (d) partially slotted cover (low AC rate) (Pesce et al., 2007).
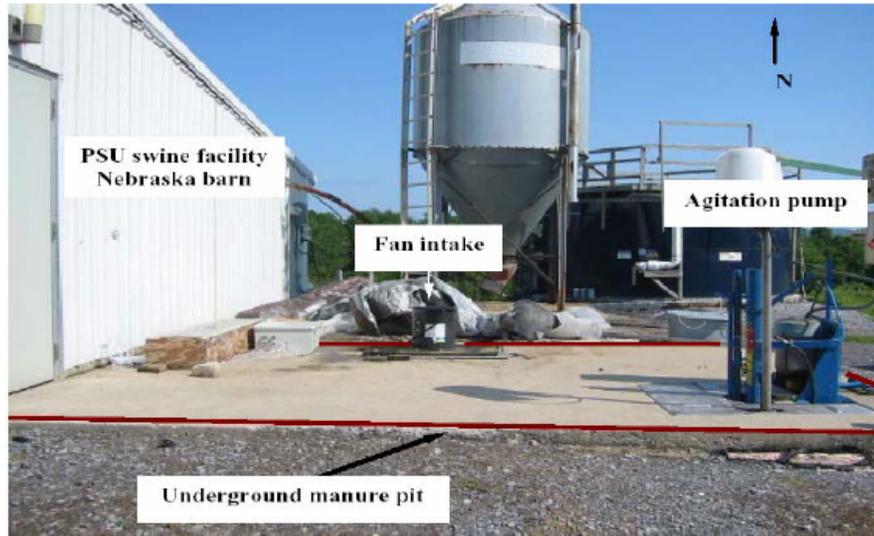
Figure 2. Experimental system for the extended validation studies.

In this research, the CFD model was used to simulate the unsteady-state gas concentration decrease during forced ventilation to identify the time taken to reach the OSHA permissible exposure limit of 10 ppm for H_2S (T_{pel}). Momentum effects were much greater than buoyancy effects within the fan-ventilated confined-space manure storage airspace in this study. In addition, the difference between the outside air temperature and the air temperature in the storage was small ($<3°C$). Therefore, for the CFD model, the gas (i.e., H2S) was assumed incompressible with constant density.

CFD CODE PERFORMANCE VERIFICATION

Since PHOENICS is a commercial CFD code, it is necessary to verify whether the CFD code is capable of simulating H_2S concentration decrease during forced ventilation in confined-space storages. The CFD code verification was performed for the following aspects: basic flow feature and assessing the CFD applications, as suggested by Srebric and Chen (2002). Three mathematical concepts are useful in determining the success of the numerical methods of the CFD model: convergence, consistency, and stability (Versteeg and Malalasekera, 1995). In this research, extensive grid-dependence and time-step sensitivity studies were conducted to ensure convergence, consistency, and stability of the numerical methods of the CFD model. Detailed verification of the CFD code is presented by Zhao (2006). These efforts demonstrated that the CFD simulation captured the major characteristics of the gas decay during forced ventilation and that the CFD code is capable of performing simulations of gas concentration decrease in the confined-space manure storages during forced ventilation (Zhao, 2006).

GRID-DEPENDENCE AND TIME-STEP SENSITIVITY STUDIES
Grid-Dependence Study

In the PHOENICS CFD code (CHAM, 2005), the finite volume method is the numerical method used to solve the transport equations (Versteeg and Malalasekera, 1995). The first step in the finite volume method is to divide the computational domain into discrete control volumes. A number of nodal points are positioned within the domain and near the boundary of the domain, and each node is surrounded by a control volume or cell (grid). The equations are solved for each node within the control volume. The size of the grid should be fine enough to ensure a high-quality solution of the governing equations. A high-quality solution of the governing equations is capable of describing the real physical process.

A grid-dependence study is performed to eliminate errors due to the coarseness of a grid. In this procedure, an initially coarse grid is refined until certain key results (e.g., fluid velocity) do not change significantly (difference <5%) between successively denser grid patterns. When key results do not change significantly, the simulation is considered grid independent. However, Sørensen and Nielsen (2003) noted that "because of restriction in computer power and time, obtaining a grid-independent solution is almost impossible, at least for three-dimensional calculations." Therefore, the grid should be refined until the key results do not change significantly (difference <5%) between successively denser grid patterns to preserve confidence in solutions. In addition, the increase in computing time with the refinement of the grid should be considered as well.

Since the geometry of the simulated manure tank was simple (rectangular), a structural grid was used. The computational domain (manure tank) was divided into several regions in the X, Y, and Z directions. These regions were created automatically to match the edges of each object in the domain. The grid lines were distributed uniformly in each region in each coordinate direction except in the fan area (i.e., the jet region). Since the fan was the only momentum source of the computational domain, a finer grid was used over the full storage depth in the fan area. Figure 3 shows the grid profiles in the X-Z plane (along longitudinal centerline) for the rectangular manure tank with the three cover types at the high and low air exchange rates and for the independent manure reception pit. A systematic refinement of the grid was conducted in the length (X), width (Y), and height (Z) directions, respectively. When the refined grid pattern satisfied the following criteria, the grid density was regarded as sufficient for the simulation case:

- Simulation results (air velocity profile) did not change significantly (<5%) with further refinement of the grid.
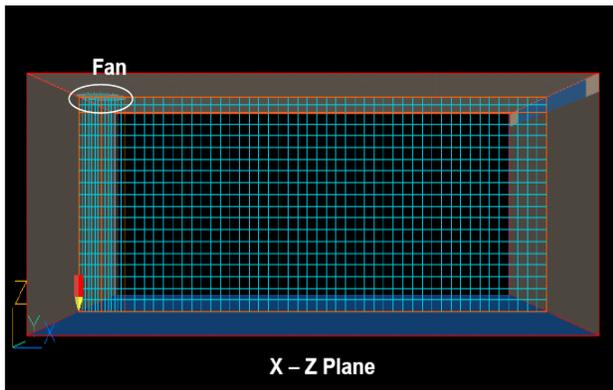
(a) Solid cover (high and low air exchange rates)
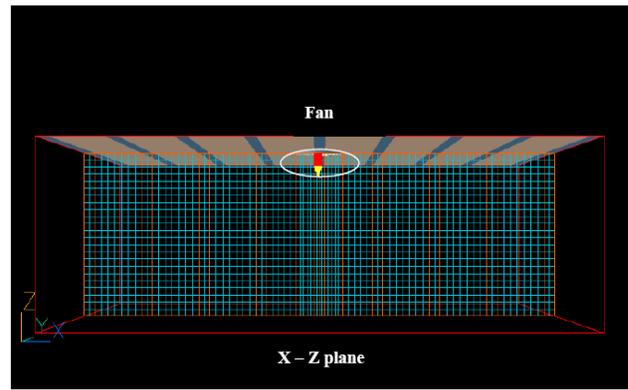
(b) Fully slotted cover (high and low air exchange rates
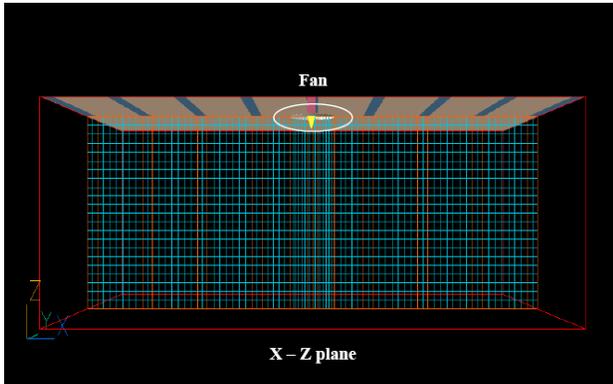
(c) Partially slotted cover (high air exchange rate)
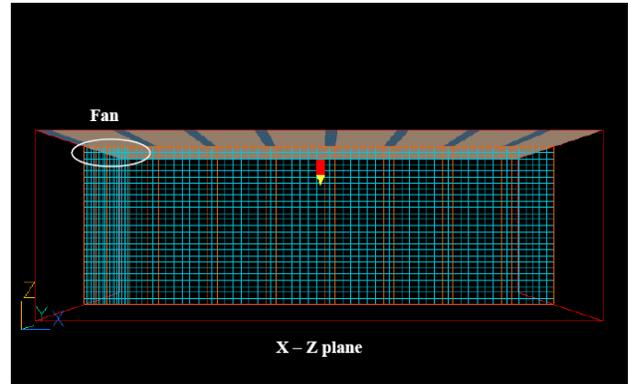
(d) Partially slotted cover (low air exchange rate)
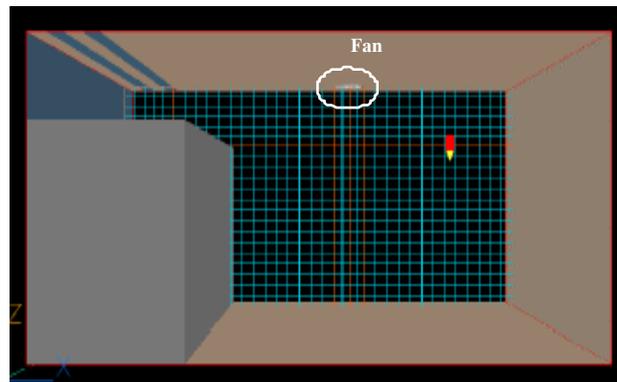
(e) Independent manure reception pit

Figure 3. Grid profiles in *X–Z* planes for (a) solid, (b) fully slotted, (c and d) partially slotted cover types, and (e) independent manure reception pit (PHOENICS 3.6; CHAM, 2005).

- The difference between simulated and measured air velocity was within 10%.
- Computing time corresponding to the candidate grid density was in a reasonable range (i.e., <24 h).

Time-Step Sensitivity Study

Once the optimal grid density was identified for each cover type, the proper time step was determined for that grid density by a time-step sensitivity study. For each cover type, four candidate time steps ($\Delta t = 10$ s, $\Delta t = 15$ s, $\Delta t = 20$ s, and $\Delta t = 30$ s) were selected, and corresponding CFD simulations were conducted. The following criteria were considered for determining the candidate time steps: (1) computation time and (2) time scale used for collecting concentration data. The initial conditions and boundary conditions (i.e., initial H_2S concentration throughout the entire storage, H_2S emission rate, and H_2S concentration in inflow air) measured by Pesce et al. (2007) and this research (Zhao et al., 2007) were used to perform simulations. The simulated results for each candidate time step were compared to the measured results to identify the proper time step to ensure the accuracy of the CFD simulation. Computation time was also considered in selection of the time step.

METHODOLOGY FOR VALIDATING CFD MODELING PROTOCOLS

The simulated and measured results for the best ventilation strategies for the rectangular confined-space manure storage with each of the three cover types (fig. 1) were compared for each sampling location shown in figure 4 to validate the CFD modeling protocols. In addition, the validated CFD modeling protocols were further validated using the previously described independent manure reception pit (fig. 2). The comparisons were conducted for the following ventilation times: T_{pel}, T_{50}, T_{25}, and T_{10}. The measured datasets used to conduct comparisons were reported by Pesce et al. (2007) and Zhao (2006) for three replicates. The detailed dataset tables, which include mean measured evacuation time values, maximum time values, and minimum time values for each cover and ventilation strategy, were summarized by Zhao (2006). The mean measured time values were used for primary comparisons.

SIMULATION CASE DESCRIPTIONS AND BOUNDARY CONDITIONS

The computational domain represents the rectangular confined-space manure tank used for identifying the best ventilation strategies for the three cover types investigated in previous research (fig. 1). The size of the manure tank is 5.49 m (L) × 2.74 m (W) × 1.83 (H). For the fully slotted and partially slotted covers, each slot size is 0.03 m. Since it was hard to obtain convergent simulation results when these narrow slots were used as the boundary conditions (outlets), every set of four of these slots was combined into one larger slot to simplify the simulation boundary conditions. However, the slots were uniformly distributed along the storage cover length to represent the real boundary condition. The sampling inlet locations at which simulated and measured results were compared to validate the CFD modeling protocols are shown in figure 4.
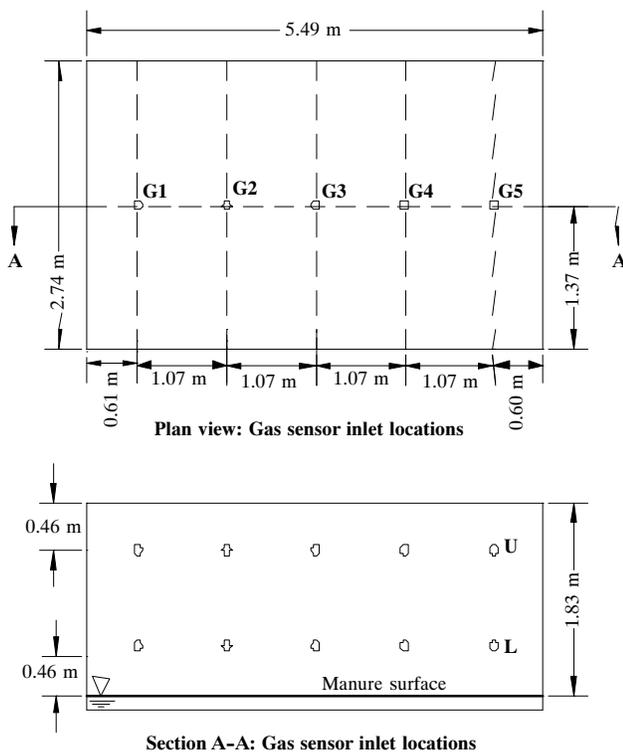
Figure 5 is a schematic diagram of the independent manure reception pit for extendedly validating the CFD modeling protocols. During measurements, the clear space above the manure was 2.29 m. The manure collected from the swine barn was flushed from the pit under the slotted cover into this underground reception pit through a 0.61 m deep manure sluice located under the slotted cover inside the barn. The sluice functioned as the primary air outlet during the pit ventilation experiments. The fan for blowing the fresh air into this confined-space pit was located above the manhole. In addition, figure 5 shows sampling inlet locations within the manure reception pit at which simulated and measured results were compared to extendedly validate the CFD modeling protocols.

Initial and Boundary Conditions

The initial condition for each simulation case shown in figure 1 and for the independent manure reception pit was the initial concentration of H_2S in the confined airspace. The boundary conditions for each simulation case illustrated in figure 1 and for the independent manure reception pit (fig. 2) included the pollutant source (liquid manure), the air inlet (fan), the walls (smooth wall with zero slide velocity in the X and Y directions), and the outlets (vent slots or cover slots). The pollutant (H_2S) source was liquid manure stored on the bottom of the confined-space manure storages. The emission rate of H_2S from the manure was expressed using a non-linear model defined from H_2S emission studies (Zhao et al., 2007), and was used to represent pollutant source strength. Unique expression for H_2S emission rates were reported for each combination of three temperature regimes (i.e., hot: $t > 18°C$, mild: $13°C < t < 18°C$, and cold: $t < 13°C$) and two ventilation air exchange rates (5 AC min^{-1} and 3 AC min^{-1}).

Figure 4. Schematic diagram of sampling inlet locations along longitudinal centerline (A-A).
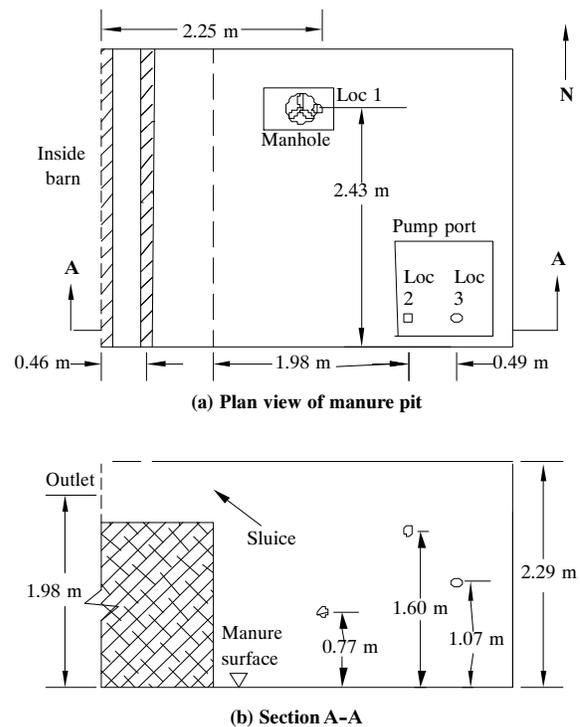
Figure 5. Schematic diagram of manure reception pit and sampling inlet locations.

Table 1. Wind speed and direction records for test dates (PSU weather station).[a]

AC Rate[b]	Cover Type	Test Date	Wind Direction	Wind Speed (km h⁻¹)
High	Solid	13 Nov. 2004	ENE	8.0
		10 May 2006[c]	N/A	0.0
	Fully slotted	25 Oct. 2004	SE	1.0
		10 May 2006	NNE	8.0
	Partially slotted	17 Nov. 2004	SW	4.2
		10 May 2006	N/A	0.0
Low	Solid	14 Nov. 2004	SWS	1.6
		10 May 2006	N/A	0.0
	Fully slotted	24 May 2004	WSW	24.0
		10 May 2006	NNE	8.0
	Partially slotted	19, 21 Nov. 2004	N	0.8
		10 May 2006	N/A	0.0

[a] Weather records were provided by PSU weather station on campus.
[b] High: 5 AC min⁻¹, low: 3 AC min⁻¹.
[c] The date for measuring inter-contamination ratios.

The fan was the source of fresh air coming into the confined-space manure storages. The airflow rate of the fan was used as a boundary input of the inlet. Since the fan was located at the same elevation as the outlet for the simulation cases, inter-contamination (the process by which a portion of exhausted contaminant gas enters a ventilated confined airspace through the fresh air intake) in inflow air was considered as an important boundary condition as well. The inter-contamination was quantified by the ratio of contaminant concentration in the inflow air to the contaminant concentration in the air exhausted from the outlet. The experimental measurements of inter-contamination for three cover types were presented by Zhao et al. (2007) (solid: 0.24, fully slotted: 0.28, and partially slotted: 0.28). For the solid cover type, the ventilation outlet was located at the east end-wall. For the fully slotted and partially slotted cover types, the slots on the cover surface were treated as outlets. For the independent manure reception pit, the manure sluice functioned as a primary outlet. External wind speed was assumed to be zero in the vicinity of the boundary of the storages in order to simplify the already complex boundary conditions in this research. However, this simplification was conservative (simulated time to reach OSHA PEL will be larger than actual) because non-zero wind speed would tend to enhance, rather than inhibit, the removal of noxious gases from the manure storage.

Inter-Contamination Adjustment

Table 1 lists wind velocity and direction on the test dates for measuring inter-contamination ratio (10 May 2006) and the test dates for collecting gas decay data for the best ventilation strategies identified for the three cover types ventilated at the high and low AC rates. For the low AC rate, the wind velocities on the respective test dates for the gas concentration decrease and inter-contamination ratio measurements were similar (difference <2 km h⁻¹) for the solid and partially slotted cover cases. For these cases, the measured inter-contamination ratios were used as boundary conditions. For the high AC rate, the wind velocity differences (4 to 8 km h⁻¹) on the respective tests dates were much higher for all cover cases. Thus, adjustments to measured inter-contamination
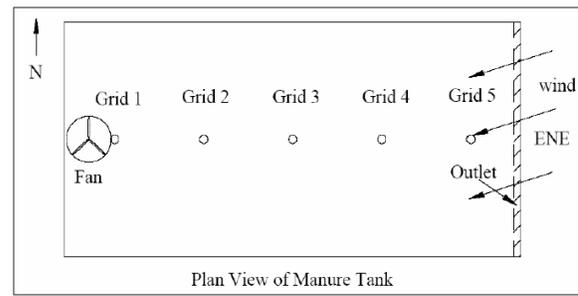
(a) Solid cover
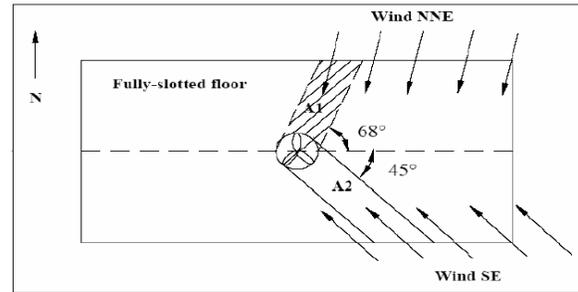
(b) Fully slotted cover
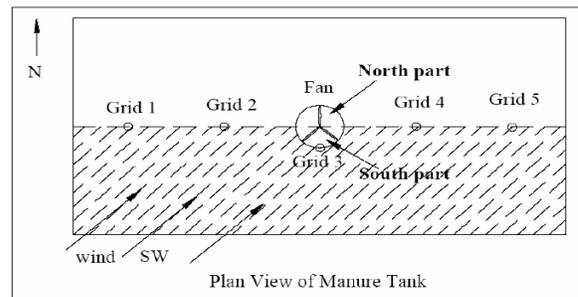
(c) Partially slotted cover

Figure 6. Wind direction for (a) solid cover, (b) fully slotted cover, and (c) partially slotted cover (high AC rate) on validation test dates.

ratios were needed to characterize the system boundary conditions for the three cover cases. For the fully slotted cover case at the low AC rate, the wind velocity on the date for collecting gas concentration decrease data was very high (24 km h⁻¹), and the wind velocity difference between respective test dates for collecting the gas concentration decrease data and measuring the inter-contamination ratio was very large (difference = 16 km h⁻¹). The combination of high wind velocity for the gas concentration decrease measurement data and the totally slotted cover most likely produced a boundary condition with reduced gas contamination concentration directly above the storage tank. Thus, simulations were conducted for a zero inter-contamination boundary and for a boundary condition with the inter-contamination ratio reported by Zhao et al. (2007) for the fully slotted cover case ventilated at the low AC rate.

Figure 6 shows schematic diagrams of the wind directions on test dates for collecting H_2S concentration decay data and for measuring inter-contamination ratios for the solid cover case (fig. 6a), the fully slotted cover case (fig. 6b), and the partially slotted cover case (fig. 6c) at the high AC rate. Based on figure 6, a quantitative analysis of the effects of wind velocity and direction on the inter-contamination ratio for the

three cover cases was conducted to obtain the wind-effect adjusted inter-contamination ratios.

For the solid cover case, an 8 km h^{-1} wind with an east-northeast (ENE) direction had momentum to move an increased volume per unit of time of contaminant-laden air (Q) exhausted from the outlet into the fan intake. The increasing percentage of the volumetric flow rate [$(Q_0 - Q)/Q_0$] due to the wind velocity and direction was used to adjust the corresponding measured inter-contamination ratio. Equation 1 was used to calculate the adjusted inter-contamination ratio considering wind effect for the solid cover case. For the fully slotted cover case, the ratio of the effective slotted cover areas (area from which the wind brings contaminant-laden air exhausted from the slots to the fan intake) for the wind directions of the test dates for collecting the gas decay data (A_2) and for measuring the inter-contamination ratio (A_1) (10 May 2006) was used to adjust the corresponding measured inter-contamination ratio. The equation for adjusting the measured inter-contamination ratio is presented in equation 2 for the fully slotted cover case. For the partially slotted cover case, the ratio of effective slotted cover areas (areas from which the wind of SW direction brings the contaminant-laden air exhausted from the slots to the fan intake) and the quantitative effect of non-zero wind momentum on the volumetric flow rate (Q) of the contaminant-laden air into the fan intake were calculated to adjust the corresponding measured inter-contamination ratio. Equation 3 was used to obtain the adjusted inter-contamination ratio considering wind effects:

$$IC_{adj.} = IC_{meas.} \times \left| \frac{Q_0 - Q}{Q_0} \right| \qquad (1)$$

$$IC_{adj.} = IC_{meas.} \times \frac{A_2}{A_1} \qquad (2)$$

$$IC_{adj.} = IC_{meas.} \times \frac{Q}{Q_0} \qquad (3)$$

where

$IC_{adj.}$ = adjusted inter-contamination ratio considering wind effect

$IC_{meas.}$ = measured inter-contamination ratio

Q_0 = volumetric airflow rate through the fan intake (high AC rate: 2.67 m^3 s^{-1})

Q = volumetric airflow rate considering wind effect (m^3 s^{-1})

A_1 = effective slotted cover of wind on the date of measuring inter-contamination ratio (m^2)

A_2 = effective slotted cover of wind on the date of collecting gas decay data (m^2).

Table 2 lists the measured and adjusted inter-contamination ratios for the three cover cases. Detailed calculations of inter-contamination ratio adjustments are presented by Zhao (2006). The adjusted inter-contamination ratios given in table 2 were used to perform CFD simulations for the three cover cases at the high AC rate.

The inter-contamination ratio for the extended validation manure reception pit was measured using the same methods presented by Zhao et al. (2007) for the rectangular manure tank. These tests were conducted on the same day as the gas decay data were collected; thus, the measured inter-contamination ratio of 0.54 was used directly as a boundary condition for the CFD simulation of the reception pit.

Table 2. Measured and adjusted inter-contamination ratios for the three cover cases at high air exchange rate.

Cover Type	Inter-contamination Ratio	
	Measured	Adjusted
Solid	0.24	0.30
Fully slotted (high AC rate)	0.28	0.42
Partially slotted	0.28	0.68

STATISTICAL CRITERIA FOR THE CFD MODELING PROTOCOLS VALIDATION

The validation criteria published in ASTM Standard D 5157-97 (ASTM, 2003) were used as the reference validation criteria in this research. The criteria recommended by ASTM D 5157-96 are: (1) correlation coefficient of 0.9 or greater, (2) regression slope between 0.75 and 1.25, (3) regression intercept 25% or less of the average measured concentration, (4) normalized mean square error (NMSE) of 0.25 or lower, (5) fractional bias of the mean concentrations of 0.25 or lower, and (6) fractional bias based on the variance of the concentrations of 0.5 or lower. The ASTM criteria were developed for highly controlled experimental systems. Since the experiments for validation were conducted using a real on-farm manure tank, the experimental system was exposed to many uncontrollable, real-world factors such as natural wind effects and construction imperfections. Therefore, the ASTM D 5157-97 criteria were used in this research with some relaxations (i.e., only the first three criteria were used) to evaluate the regression of simulated and measured results. An additional statistical criterion imposed by the authors for successful simulations was that the difference between the simulated and measured time to reach the OSHA PEL for H$_2$S was less than or equal to 10%.

RESULTS AND DISCUSSIONS

GRID-DEPENDENCE AND TIME-STEP SENSITIVITY STUDIES

Rectangular Manure Tank Computational Grid

Table 3 summarizes candidate grid densities (from coarse grid to fine grid) for the best ventilation strategy identified for each cover type and for the ventilation configuration of the independent manure reception pit. Here, grid density represents the grid numbers in the X, Y, and Z directions. The corresponding computing time to solution convergence for each grid density is listed in table 3 as well.

For the solid cover type and for both the high and low AC rates, the simulated velocities at the area inside the fan jet zone began to converge (difference <5%) when the grid was refined to 45 × 34 × 16. For the fully slotted cover type at both the high and low AC rates, when the grid density was refined to 60 × 32 × 18, the simulated results began to converge (difference <5%). For the partially slotted cover type at the high AC rate, convergence occurred when the grid density was refined to 58 × 32 × 18. For the partially slotted cover type at the low AC rate, the simulated result converged when the grid density was refined to 56 × 32 × 20. In addition, the convergence conditions in the areas outside the fan jet zone were checked. The grid densities that yielded the best convergence both within and outside the fan jet zone for the three cover cases at the two AC rates were 58 × 46 × 19 for the solid cover case at both the high and low AC rates, 82 × 40 × 23 for the fully slotted cover case at both the high and low AC rates, 79 × 44 × 26 for the partially slotted cover

Table 3. Summary of candidate grid densities and computing times to solution.

Cover Type	AC Rate[a]	Candidate Grid Density[b]	Computing Time (min)
Solid	High	45 × 34 × 16	55
		54 × 42 × 18	95
		58 × 46 × 19	110
		63 × 50 × 20	127
		67 × 54 × 22	151
	Low	45 × 34 × 16	60
		54 × 42 × 18	70
		58 × 46 × 19	90
		63 × 50 × 20	120
		67 × 54 × 22	160
Fully slotted	High	60 × 32 × 18	40
		74 × 34 × 21	65
		82 × 40 × 23	100
		94 × 44 × 25	160
		96 × 46 × 27	175
	Low	58 × 30 × 18	37
		74 × 34 × 21	60
		82 × 40 × 23	110
		94 × 44 × 25	160
		96 × 46 × 27	175
Partially slotted	High	58 × 32 × 18	40
		66 × 36 × 20	62
		86 × 44 × 22	130
		90 × 46 × 26	171
	Low	56 × 32 × 20	45
		73 × 40 × 23	86
		79 × 44 × 26	114
		85 × 46 × 30	196
		92 × 50 × 34	208

[a] High: 5 AC min-1, low: 3 AC min-1.
[b] Grid density represents cell numbers in length (*X*), width (*Y*), and height (*Z*) directions, respectively.

case at the low AC rate, and 86 × 44 × 22 for the partially slotted cover case at the high AC rate.

The simulated air velocities obtained based on the grid densities identified were then compared to measured values at the fan surface to ensure that these grid densities were sufficient to perform high-quality CFD simulations. Figure 7 is a schematic diagram of the fan surface and velocity measuring locations. The comparisons were conducted for locations 1,
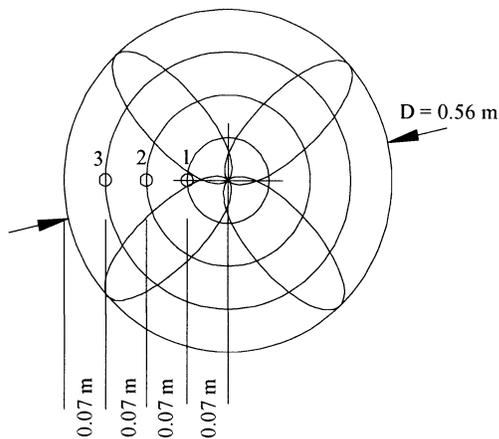
Figure 7. Schematic diagram of fan surface and velocity measuring locations.

Table 4. Simulated and measured velocity values at locations 1 to 3 for three cover cases for two air exchange rates.

Location	Cover Type	AC Rate[a]	Grid Density	Velocity (m s-1)[b] Sim.	Velocity (m s-1)[b] Meas.	Diff. (%)
1	Solid	High	58×46×19	12.1	12.3	-2
		Low	58×46×19	7.0	7.2	-3
	Fully slotted	High	82×40×23	11.7	12.3	-5
		Low	82×40×23	6.7	7.2	-7
	Partially slotted	High	86×44×22	11.4	12.3	-7
		Low	79×44×26	6.8	7.2	-6
2	Solid	High	58×46×19	12.1	12.5	-3
		Low	58×46×19	7.0	7.5	-7
	Fully slotted	High	82×40×23	11.8	12.5	-6
		Low	82×40×23	6.7	7.5	-10
	Partially slotted	High	86×44×22	11.4	12.5	-9
		Low	79×44×26	6.8	7.5	-9
3	Solid	High	58×46×19	12.1	12.6	-4
		Low	58×46×19	7.0	7.1	-1
	Fully slotted	High	82×40×23	11.8	12.6	-6
		Low	82×40×23	6.7	7.1	-6
	Partially slotted	High	86×44×22	11.4	12.6	-10
		Low	79×44×26	6.8	7.1	-4

[a] High: 5 AC min-1, Low: 3 AC min-1.
[b] Sim. = simulated, Meas. = measured, and Diff. = difference between measured and simulated velocity values.

2, and 3. The differences between the simulated and measured velocity values were all less than or equal to 10% (table 4); therefore, the selected grid densities were sufficient to ensure the accuracy of the CFD simulations.

Rectangular Manure Tank Time-Step Sensitivity

Table 5 lists simulated and measured T_{pel} values for each candidate time step for five sampling inlet locations (grid 1 to grid 5, upper and lower levels, fig. 4) for the solid cover case. The measured T_{pel} shows the range obtained from three replicates. The simulated T_{pel} values obtained using time steps of 10 s and 15 s fall within 10% difference of the average measured values. The simulated T_{pel} values obtained using time steps of 20 s and 30 s overpredict the average measured values at grid 2 to grid 5 of the lower level (>10%). Therefore, time steps of 10 s and 15 s were satisfactory for further solid cover simulations. Versteeg and Malalasekera (1995) noted that a small time step was needed for the fully implicit scheme to ensure the accuracy of the CFD simulations. Thus, the time step of 10 s was selected for performing the CFD simulations for the grid density of 58 × 46 × 19.

Table 6 summarizes simulated and measured T_{pel} values of sampling inlet locations for each candidate time step for the fully slotted cover case. For the fully slotted cover case, the measured results were for three sampling locations along the tank width at grid 1. Based on the agreement between measured and simulated T_{pel} and the required computing time, the time step of 10 s was identified as being appropriate for the corresponding grid density (82 × 40 × 23) for the fully slotted cover case.

Table 5. Measured and simulated T_{pel} values (s) for candidate time-steps for the solid cover case ventilate at 3 AC min^{-1} (C_0 = 142.9 ppm).

	Δt (s)				Measured T_{pel},[a] (Range), and Mean
	10	15	20	30	
Grid 1					
Upper level	50	50	56	62	(57, 66), 62
Lower level	52	53	58	65	(59, 63), 61
Grid 2					
Upper level	53	54	60	67	(55, 63), 59
Lower level	56	58	64	71	(59, 64), 61
Grid 3					
Upper level	54	55	60	67	(52, 60), 56
Lower level	61	63	76	87	(55, 65), 60
Grid 4					
Upper level	57	59	64	72	(45, 65), 57
Lower level	66	68	76	87	(59, 69), 64
Grid 5					
Upper level	63	65	71	82	(46, 62), 54
Lower level	73	76	90	100	(64, 74), 69
Computing time	10.5 h	7.2 h	5.5 h	4 h	

[a] The range of measured T_{pel} values represents the maximum and minimum measured T_{pel} values for three replicates; mean value is for three-replicate measured values; grid density: $58 \times 46 \times 19$.

Table 7. Measured and simulated T_{pel} values (s) for candidate time-steps for the partially slotted cover case ventilate at 3 AC min^{-1} (C_0 = 97.0 ppm).

	Δt (s)				Measured T_{pel},[a] (Range), and Mean
	10	15	20	30	
Grid 1					
Upper level	62	67	70	78	(62, 77), 70
Lower level	70	73	77	85	(62, 91), 80
Grid 2					
Upper level	74	79	84	93	(69, 75), 73
Lower level	77	82	86	95	(58, 84), 74
Grid 3					
Upper level	84	87	93	103	(66, 80), 73
Lower level	88	93	99	109	(64, 86), 77
Grid 4					
Upper level	89	94	99	109	(65, 78), 73
Lower level	94	100	106	117	(60, 96), 82
Grid 5					
Upper level	88	94	99	109	(62, 82), 72
Lower level	99	98	104	115	(54, 90), 78
Computing time	20.5 h	15 h	13 h	9 h	

[a] The range of measured T_{pel} values represent the maximum and minimum measured T_{pel} values for three replicates; mean value is for three-replicate measured values grid density: $79 \times 44 \times 26$.

Table 7 lists simulated and measured T_{pel} values of sampling inlet locations for each candidate time step for the partially slotted cover case. With the exception of grid 1, the simulated T_{pel} values for the time step of 10 s fall within 10% of the average measured T_{pel} values at grid 2 to grid 5 for both the upper and lower levels. At grid 1, simulated T_{pel} values were within 15% of the average measured T_{pel} values for both the upper and lower levels. For this case, the sampling inlet location at grid 1 was closest to the fan (jet zone). The high velocity gradient could lead to small inaccuracies of the simulated results or larger measurement errors due to small inaccuracies in measuring station locations in the vicinity of grid 1. Considering these potential error sources in the high velocity gradient in the jet region (i.e., grid 1), and since the simulated T_{pel} values were still within 15% of the mean measured T_{pel} values (average of three replicates), the time step

of 10 s is deemed acceptable for the selected grid density ($79 \times 44 \times 26$).

Independent Manure Reception Pit

Tables 8a and 8b list candidate grid densities, computing times, and simulated mean velocities at locations inside and outside the fan jet zone for each candidate grid density for the independent reception pit. The simulated results began to converge when the grid density was refined to $36 \times 29 \times 21$ inside and outside the fan jet zone. Table 9 lists the simulated and measured air velocities at three locations at the fan surface (fig. 7). The difference between the simulated and measured air velocities was within 10% (locations 1 and 3) when the grid density was refined to $36 \times 29 \times 21$. Considering the

Table 6. Measured and simulated T_{pel} values (s) for candidate time-steps for the fully slotted cover case ventilate at 3 AC min^{-1} at grid 1[a] (C_0 = 107.3 ppm).

Grid 1	Δt (s)				Measured T_{pel},[b] (Range), and Mean
	10	15	20	30	
Location 1					
Upper level	33	34	38	42	(13, 26), 22
Lower level	32	34	36	40	(15, 42), 29
Location 2					
Upper level	33	35	38	42	(11, 32), 23
Lower level	31	33	36	40	(18, 37), 30
Location 3					
Upper level	33	34	38	42	(26, 32), 23
Lower level	32	34	36	40	(17, 42), 33
Computing time	8.5 h	6.5 h	4.4 h	4.4 h	

[a] The measurements were conducted for three locations at grid 1 on the same test date (Pesce, 2005); therefore, the simulations results used are for three locations at grid 1 as well.

[b] The range of measured T_{pel} values represent the maximum and minimum measured T_{pel} values for three replicates; mean value is for three-replicate measured values; grid density: $82 \times 40 \times 23$.

Table 8a. Mean velocities in the fan jet at $X : Y : Z$ = 2.41 m : 2.57 m : 1.98 m and computing times for selected grid densities for the extended validation case.

Grid Density	Computing Time (h)	Mean Velocity (m s^{-1})	Difference[a] (%)
$32 \times 25 \times 17$	0.4	5.4	-25
$34 \times 27 \times 19$	1	7.0	0
$36 \times 29 \times 21$	1	7.0	0
$38 \times 31 \times 23$	1.1	7.0	0

[a] The difference is calculated based on the value of finer grid density (i.e., $38 \times 31 \times 23$).

Table 8b. Mean velocities outside the fan jet at $X : Y : Z$ = 3.48 m : 2.57 m : 1.98 m and computing times for selected grid densities for the extended validation case.

Grid Density	Computing Time (h)	Mean Velocity (m s^{-1})	Difference[a] (%)
$32 \times 25 \times 17$	0.4	0.13	-13
$34 \times 27 \times 19$	1	0.13	-13
$36 \times 29 \times 21$	1	0.15	0
$38 \times 31 \times 23$	1.1	0.15	0

[a] The difference is calculated based on the value of finer grid density (i.e., $38 \times 31 \times 23$).

Table 9. Simulated and measured velocities at the fan surface at locations 1 to 3 for the extended validation case.

Fan Face Location[a]	Grid Density	Velocity (m s^{-1})[b] Sim.	Velocity (m s^{-1})[b] Meas.	Diff (%)
1	$32 \times 25 \times 17$	4.4	6.3	-30
	$34 \times 27 \times 19$	5.9	6.3	-6
	$36 \times 29 \times 21$	5.9	6.3	-6
	$38 \times 31 \times 23$	5.9	6.3	-6
2	$32 \times 25 \times 17$	5.3	7.9	-33
	$34 \times 27 \times 19$	7.0	7.9	-11
	$36 \times 29 \times 21$	7.0	7.9	-11
	$38 \times 31 \times 23$	7.0	7.9	-11
3	$32 \times 25 \times 17$	5.3	6.3	-16
	$34 \times 27 \times 19$	7.0	6.3	10
	$36 \times 29 \times 21$	7.0	6.3	10
	$38 \times 31 \times 23$	7.0	6.3	10

[a] Locations are defined in figure 7.
[b] Sim. = simulated, Meas. = measured, and Diff. = difference between measured and simulated velocity values.

possibility of small measurement errors, the difference of 11% between the simulated and measured air velocities at location 2 is deemed acceptable. Therefore, the selected grid density identified was sufficient to ensure the accuracy of the CFD simulations.

CFD SIMULATIONS FOR H$_2$S CONCENTRATIONS DECAY DURING FORCED VENTILATION

Figure 8 shows the simulated transient concentration contours of the cross-section along the longitudinal centerline of the rectangular confined-space manure tank for H$_2$S at the 10th second, 30th second, and 50th second after ventilation commenced. These figures show the H$_2$S concentration decay during forced ventilation for the best ventilation strategies of three cover cases. The ratio of the maximum concentration (C$_{max}$) to the initial concentration (C$_0$) is given for each time increment. The decrease of the ratio value for each time increment shows a decay trend of H$_2$S concentration during forced ventilation. The area of highest gas concentration in confined airspace for each time increment is shown in figure 8. The lowest concentration level occurred near the fan area (solid circle line).

The H$_2$S concentration decrease over time is illustrated by the decreasing size of the high-concentration region. In addition, these figures demonstrate the decrease in the maximum H$_2$S concentration in the entire storage domain with ventilation time. For example, the maximum H$_2$S concentration decreased from 137.2 ppm to 25.8 ppm (difference = 82%) within 50 s for the solid cover case (fig. 8a), the maximum concentration decreased from 29.2 ppm to 7.4 ppm (difference = 75%) within 50 s for the fully slotted cover case (fig. 8b), and the maximum concentration decreased from 92.8 ppm to 35.2 ppm (difference = 6%) within 50 s for the partially slotted cover case (fig. 8c). Based on the quantitative concentration decrease trends for the three cover types, forced ventilation is clearly an effective method to remove noxious gas from the confined-space manure storages.

The H$_2$S concentration contours also identify the zones of the high gas concentration for the ventilation case for each cover type. For the solid and the partially slotted cover types, the fan was located at the midpoint of the west end-wall. Therefore, the gas concentration in the zone closest to the fan was lower than in the zone farther from the fan (i.e., the cor-

t = 10 s, C$_{max}$/C$_0$ = 0.96
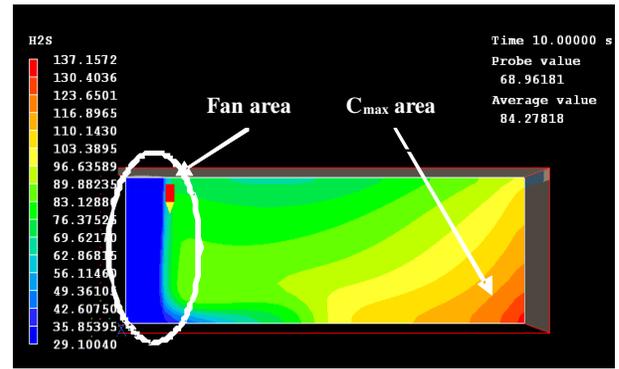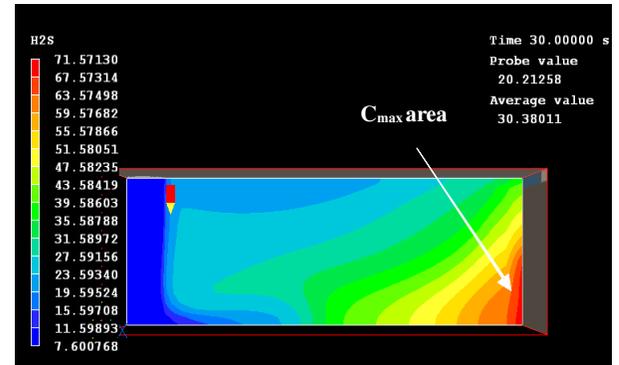
t = 30 s, C$_{max}$/C$_0$ = 0.50
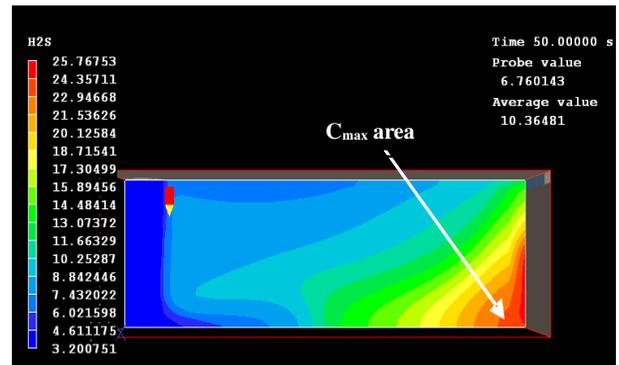
t = 50 s, C$_{max}$/C$_0$ = 0.18

Figure 8a. H$_2$S concentration decay contours with solid cover (C$_0$ = 142.9 ppm).

ner at the bottom of east end-wall). It took longer to reduce H$_2$S concentration to OSHA PEL in the zone farthest from the fan. For the fully slotted cover type, the fan was located at the midpoint of the top cover, and it divided the air space into two symmetric parts in the longitudinal direction. A high gas concentration zone is shown in the area within the vortex generated by the entrainment effect of the fan on the surrounding fluid. These visualized features help identify potentially unsafe zones when entering a ventilated confined-space manure storage facility.

VALIDATION OF THE CFD MODELING PROTOCOLS

This section presents the results of the simulations for the rectangular manure tank defined in figure 1 for solid, fully

t = 10 s, $C_{max}/C_0 = 0.83$

t = 10 s, $C_{max}/C_0 = 0.96$

t = 30 s, $C_{max}/C_0 = 0.42$

t = 30 s, $C_{max}/C_0 = 0.62$

t = 50 s, $C_{max}/C_0 = 0.21$
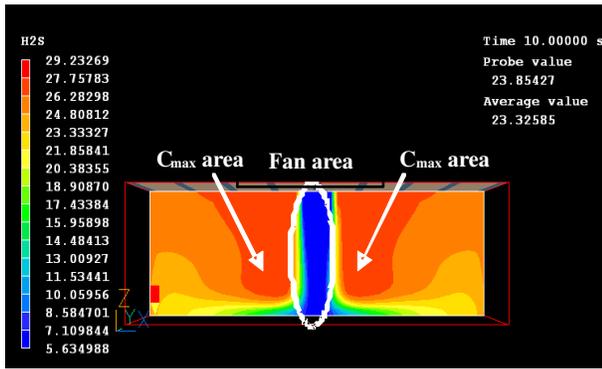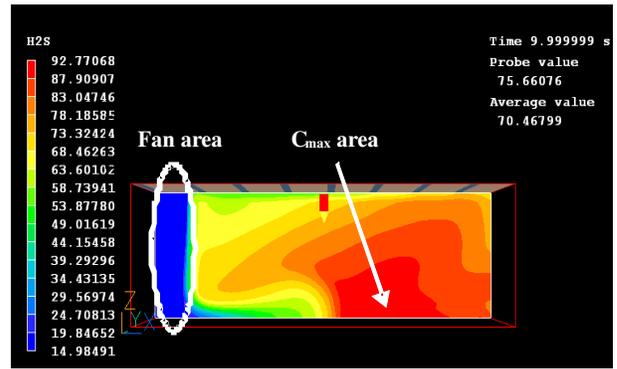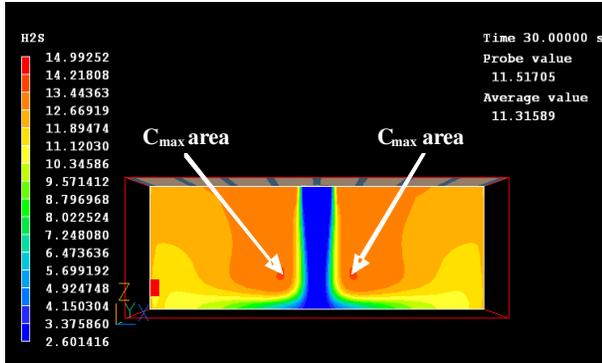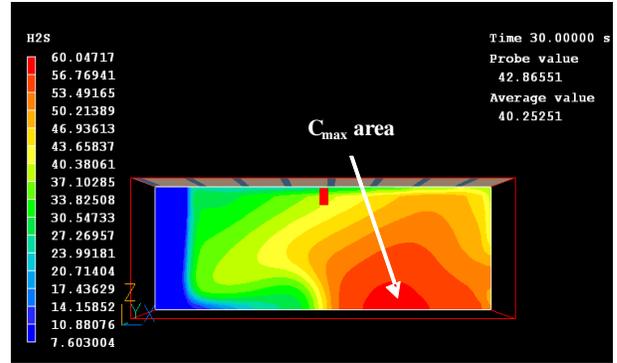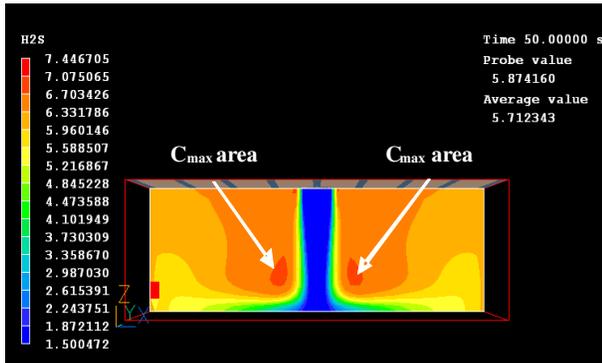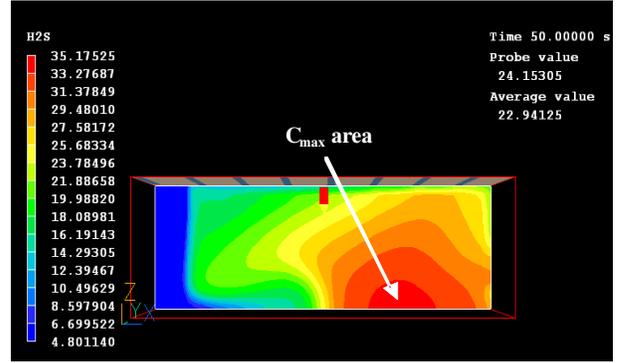
t = 50 s, $C_{max}/C_0 = 0.36$

Figure 8b. H_2S concentration decay contours with fully slotted cover ($C_0 = 35.3$ ppm).

Figure 8c. H_2S concentration decay contours with partially slotted cover ($C_0 = 97.0$ ppm).

slotted, and partially slotted covers. Included are comparisons between simulated and measured time values (i.e., T_{pel}, T_{50}, T_{25}, and T_{10}) for the three cover types at the high and low air exchange rates.

Rectangular Manure Tank with Solid Cover

Figure 9 shows comparisons between simulated and measured T_{pel} values for the five sampling locations (grid 1 to grid 5) for the high and low air exchange rates at both the upper and lower levels for the solid cover case. The mean measured T_{pel} values were used to perform primary comparisons. The standard deviation values of the measured T_{pel} at five grids at both the upper and lower levels are between 1.7 and 8.3 at the low air exchange rate and between 0.9 and 5.7 at the high air exchange rate.

For the high AC rate (fig. 9a), the T_{pel} values of grid 2 to grid 5 at the upper level and grid 5 at the lower level are within 10% of the mean measured T_{pel} values. At the lower level, the T_{pel} values of grid 2 to grid 4 are within 10% of the minimum measured T_{pel} values. However, for grid 1, the sampling location closest to the fan area (high velocity gradient), the T_{pel} value is within 10% of the minimum measured T_{pel} value at the upper level and within 22% of the minimum measure T_{pel} value at the lower level. For the low AC rate (fig. 9b), the T_{pel} values of grids 2 to 4 at the upper level and grids 2 to 5 at the lower level are within 10% of the mean measured T_{pel} values. For grid 5 at the upper level, the T_{pel} value is still within 15% of the minimum measured T_{pel} value. The T_{pel} values of grid 1 at both the upper and lower levels are underpredicted compared to the measured T_{pel} values. However, the T_{pel}

(a) High AC rate

(b) Low AC rate
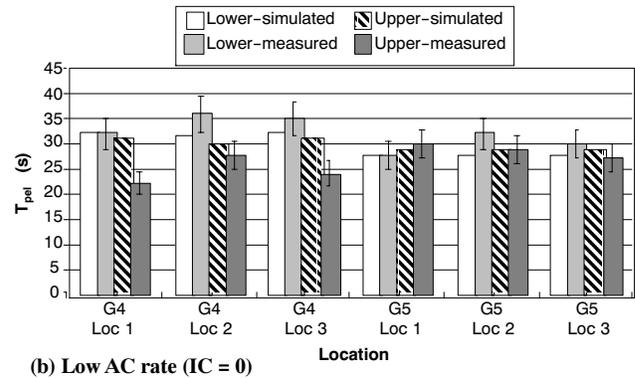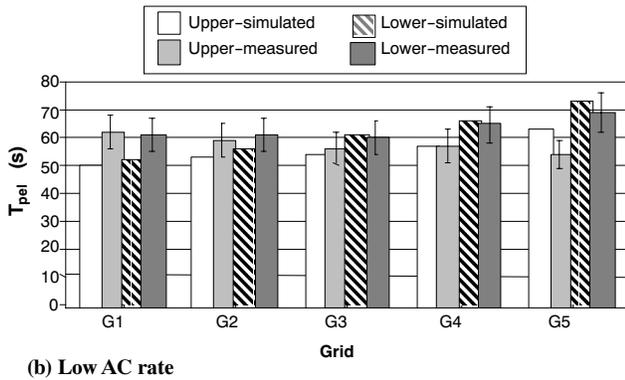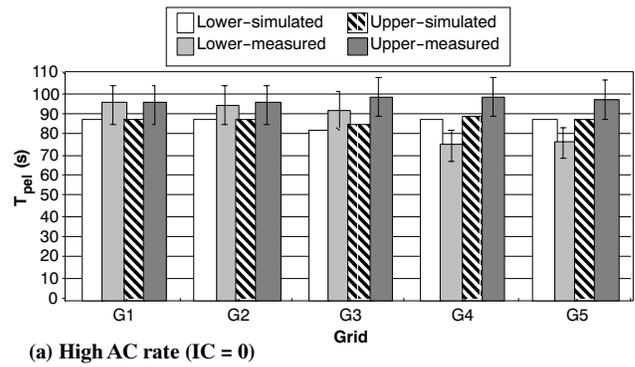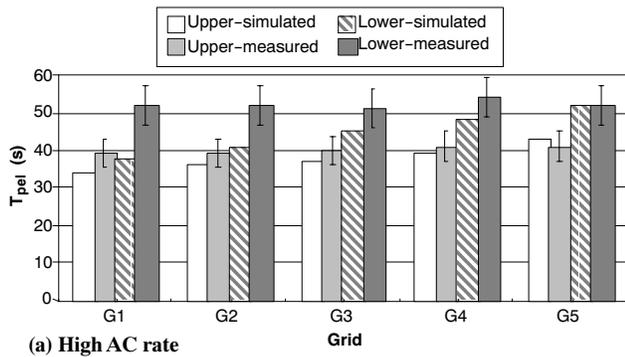
Figure 9. Simulated vs. measured T_{pel} values for the solid cover case at the upper and lower levels for both the high (adjusted inter-contamination ratio = 0.30) and low air exchange rates.

values are still within 15% and 10% of the minimum measured T_{pel} values at the upper and lower levels, respectively.

Rectangular Manure Tank with Fully Slotted Cover

Figure 10 shows comparisons between simulated and measured T_{pel} values for the five sampling locations (grid 1 to grid 5) for the high AC rate and the three sampling locations (locations 1 to 3) at grids 4 and 5 for the low AC rate at both the upper and lower levels for the fully slotted cover case. The mean measured T_{pel} values were used to perform primary comparisons. The standard deviation values of the measured T_{pel} at three locations at grids 4 and 5 at both the upper and lower levels are between 1.9 and 11.3 at the low air exchange rate. For the high air exchange rate, the standard deviation values of the measured T_{pel} at both the upper and lower levels are between 1.0 and 10.5 at the high air exchange rate.

For the high AC rate (fig. 10a) at the upper level, except grid 3, the simulated T_{pel} values at other sampling locations are within 10% of the mean measured T_{pel} values. Grid 3, the sampling location closest to the fan jet is characterized by a very high velocity gradient. This flow feature could lead to small simulation inaccuracies and measurement errors. However, the simulated T_{pel} at grid 3 is still within 15% of the minimum measured T_{pel} value. For the high AC rate at the lower level (fig. 10a), the simulated T_{pel} values at grid 1 and grid 2 are within 10% of the mean measured T_{pel} values. At grid 3 (high velocity gradient region), the measured T_{pel} is within 10% of the minimum measured T_{pel}. The simulated T_{pel} values are overpredicted at grids 4 to 5 compared to the mean measured T_{pel} values; however, they are within 15% of the mean measured T_{pel} values.

(a) High AC rate (IC = 0)

(b) Low AC rate (IC = 0)

(c) Low AC rate (IC = 0.28)
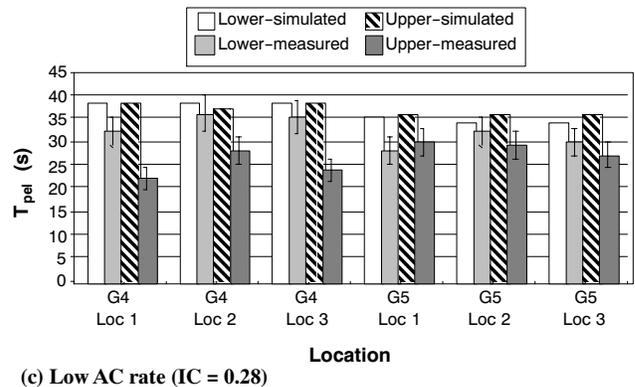
Figure 10. Simulated vs. measured T_{pel} values for the fully slotted cover case at the upper and lower levels for both the high and low air exchange rates.

For the low AC rate, figure 10b shows the comparisons between the measured and simulated T_{pel} values at the upper and lower levels with the boundary condition of zero inter-contamination ratio. Figure 10c presents the comparisons between the simulated and measured T_{pel} values at the upper and lower levels with the boundary condition of the measured inter-contamination ratio (0.28). For the zero inter-contamination boundary condition, the simulated T_{pel} values of locations 1 and 3 at grid 4 are overpredicted compared to the mean measured T_{pel} values at the upper level. In addition, the difference between the simulated and measured T_{pel} values at location 1 of grid 4 is higher (29%) than the value at location 3 (23%). The simulated T_{pel} values at other sampling locations at the lower level are within 10% of the mean measured T_{pel} values. For the boundary condition with the measured inter-contamination ratio, the comparisons between

simulated and measured T_{pel} values show that the simulated T_{pel} values of location 1 to location 3 at the upper level of grid 4 and grid 5 are all overpredicted compared to the mean measured T_{pel} values. The simulated T_{pel} values at locations 2 and 3 at the lower level of grid 4 and grid 5 are within 10% of the mean measured T_{pel}. At location 1 at the lower level of grid 4 and grid 5, the simulated T_{pel} values are within 20% of the mean measured T_{pel} values.

Rectangular Manure Tank with Partially Slotted Cover

Figure 11 shows comparisons between simulated and measured T_{pel} values for the five sampling locations (grid 1 to grid 5) for the high and low AC rates at both the upper and lower levels for the partially slotted cover case. The mean measured T_{pel} values were used to perform primary comparisons. The standard deviations of the measured T_{pel} values at five grids at both the upper and lower levels are between 2.8 and 16.7 at the low air exchange rate and between 0.5 and 9.5 at the high air exchange rate.

For the high AC rate (figs. 11a and 11b), the simulated T_{pel} values at grid 1 and grid 3 at the upper level are within 10% of the mean measured T_{pel} values. For grid 2, the simulated T_{pel} is within 10% of the maximum measured T_{pel}. At grid 4 and grid 5, the simulated T_{pel} values are overpredicted compared to the mean/maximum measured T_{pel} values. At the lower level, simulated T_{pel} values are within 20% of the mean measured T_{pel} values at grids 1, 2, 4, and 5. The unusual overprediction of simulated T_{pel} values at grid 4 and grid 5 occurred at the upper level. The measurement method was considered as a potential reason. Pesce et al. (2007) could only monitor six sampling locations at a time. Thus, for the partially slotted cover case, measurements at grid 1 to grid 3 and at grid 4 to grid 5 were conducted at different times. This measurement method resulted in different initial concentrations for the grids 1 to 3 versus grids 4 to 5 measurements. In order to normalize the effect of different initial concentration on simulated evacuation times at different sampling locations, comparisons between simulated T_{50} values and mean measured T_{50} values were performed.

Figure 11b shows the comparisons between simulated and measured T_{50} values at grid 1 to grid 5 at both the upper and lower levels at the high AC rate. At the upper level, except for grid 3, the simulated T_{50} values are within 10% of the mean measured T_{50} values. At the lower level, the simulated T_{50} values at grid 2 and grid 4 are within 10% of the mean measured T_{50} values. Although the simulated T_{50} values are underpredicted at grid 1 and grid 5 compared to the mean measured T_{50} values, the simulated values are within 15% of the minimum measured T_{50} values. Grid 3, the sampling location closest to the fan area, is characterized by a high velocity gradient. The complex flow feature in the vicinity of the fan area could lead to small simulation inaccuracies of the CFD simulations and larger measurement errors due to small inaccuracies in measuring station locations. Based on the above analyses using the mean T_{50} values, the effect of different initial concentration on simulated evacuation times was eliminated, and good agreement was identified between the simulated and measured results at grid 4 and grid 5. Therefore, the different initial concentration due to the measurement method was the probable reason for the large differences between simulated and measured T_{pel} values at grid 4 and grid 5.

For the low AC rate (fig. 11c), the comparisons show that the simulated T_{pel} values of grid 2 to grid 5 at the lower level are within 10% of the mean measured T_{pel} values. The simulated T_{pel} values of grids 2, 3, and 5 at the upper level are within 10% of the mean measured T_{pel} values. For grid 4 at the upper level, the simulated T_{pel} is overpredicted compared to the mean measured T_{pel} value. However, it is still within 15% of the maximum measured T_{pel} value. The simulated T_{pel} of grid 1 is underpredicted compared to the mean measured value, but is still within 10% of the minimum measured T_{pel}. The grid 1 sampling location is closest to the fan area; therefore, it has a very high velocity gradient. This flow feature could lead to larger inaccuracies of simulations and measurement errors in this region.

Figure 12 shows the comparisons between simulated and measured T_{pel}, T_{50}, T_{25}, and T_{10} values for both the upper
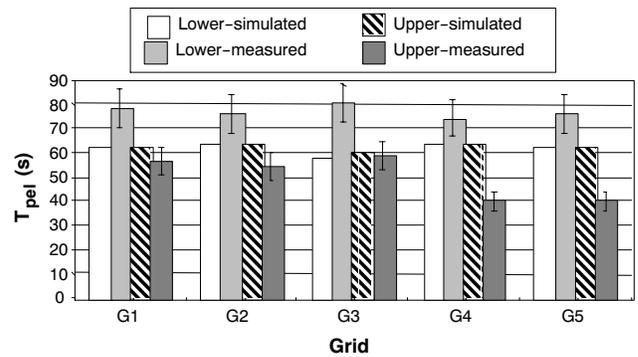
(a) High AC rate: T_{pel} values
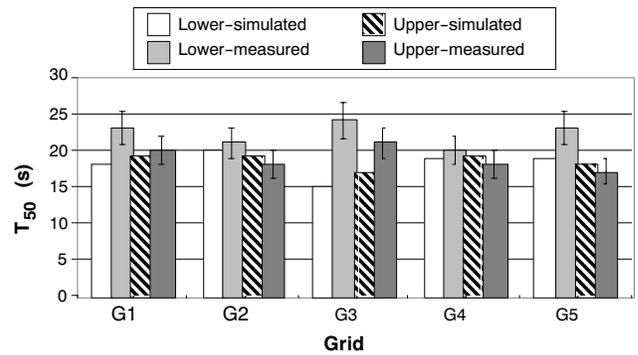
(b) High AC rate: T_{50} values
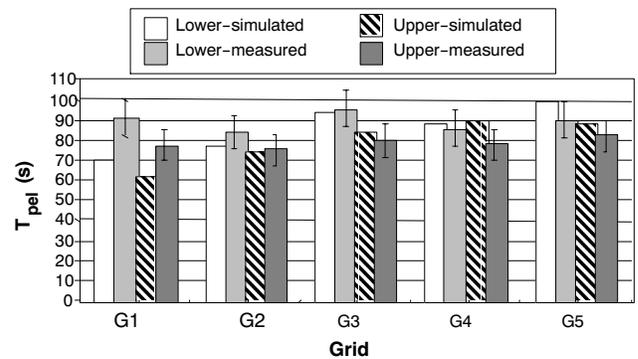
(c) Low AC rate: T_{pel} values

Figure 11. Simulated vs. measured T_{pel} and T_{50} values for the partially slotted cover case at the upper and lower levels for both the high (adjusted inter-contamination ratio = 0.68) and low air exchange rates.
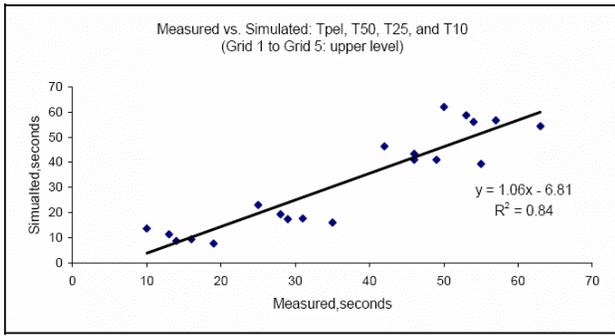
(a) Upper level
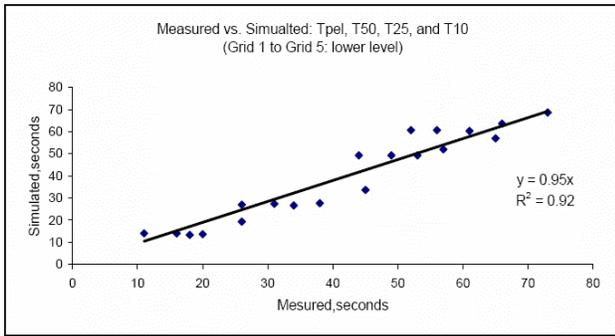
(b) Lower level

Figure 12. Simulated vs. measured T_{pel}, T_{50}, T_{25}, and T_{10} for the solid cover case at the low air exchange rate.

Table 10. Decision criteria statistics for the CFD simulations of the three cover ventilation cases at the high and low air exchange rates.

Cover Type	AC Rate[a]	Level	Correlation Coefficient >0.9	Regression Slope 0.75 ~ 1.25	Regression Intercept[c] ≤25% of Measured Value
			Statistical Criteria[b]		
Solid	High	U	0.93	1.05	1.77
		L	0.86	1.17	0.30
	Low	U	0.84	1.06	6.81
		L	0.92	0.95	0.00
Fully slotted	High	U	0.97	0.78	13.60
		L	0.93	0.84	14.29
	Low	U (IC = 0)	0.64	0.75	5.50
		U (IC = 0.28)	0.65	0.84	9.00
		L (IC = 0)	0.85	0.86	0.15
		L (IC = 0.28)	0.87	1.09	1.02
Partially slotted	High	U	0.81	0.92	4.76
		L	0.97	0.77	2.31
	Low	U	0.80	0.81	6.82
		L	0.85	0.86	4.30

[a] High AC rate: 5 AC min-1; low AC rate: 3 AC min-1.
[b] Based on the Standard Guide for Statistical Evaluation of Indoor Air Quality Model (ASTM, D5157-97).
[c] 25% of the mean measured value (T_{pel}):
Solid: high AC rate: 11 s; low AC rate: 11s.
Fully slotted: high AC rate: 22 s; low AC rate: 8 s.
Partially slotted: high AC rate: 11 s; low AC rate: 16 s.

and lower levels at the low air exchange rate for the solid cover case. The corresponding regression equations obtained for the solid cover case at the low air exchange rate are also shown in figure 12. The plots for other cover cases at both the
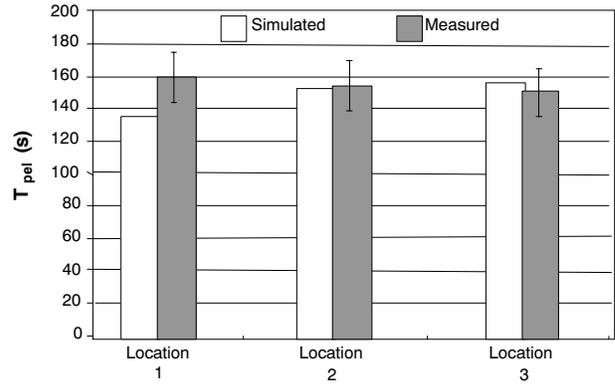
Figure 13. Simulated vs. measured T_{pel} values at three sampling locations for the extended validation case.

Table 11. Decision criteria statistics for the extended CFD modeling protocols validation at locations 1 to 3.

Location	Correlation Coefficient >0.9	Regression Slope 0.75 ~ 1.25	Regression Intercept[b] ≤25% of Measured Value
	Statistical Criteria[a]		
1 to 3	0.87	0.88	28.0

[a] Based on the Standard Guide for Statistical Evaluation of Indoor Air Quality Model (ASTM, D5157-97)
[b] The mean measured T value (T_{pel}, T_{50}, T_{25}, and T_{10}) was 89 s; therefore, 25% of the mean measured value is 22.0.

high and low AC rates showed the same trend (Zhao, 2006). The corresponding statistical evaluation of the CFD model for the three cover cases is summarized in table 10. For all the ventilation cases simulated, the slope of regression is between 0.75 and 1.25 and the intercept of regression is less than 25% of the mean measured time. The correlation coefficients of five simulated cases satisfy the statistical criterion (>0.9). Five of the simulated cases have the correlation coefficients slightly (difference <8%) less than 0.9, and only two of the simulated cases have a correlation coefficient less than 0.8 (0.64 and 0.65 for the upper level of the fully slotted cover at low AC rate with IC = 0 or IC = 0.28).

Validation Using Independent Manure Reception Pit

The comparisons between simulated and measured time values (i.e., T_{pel}, T_{50}, T_{25}, and T_{10}) were conducted for three sampling locations within the confined airspace of the manure reception pit (fig. 5). Figure 13 shows the comparisons between simulated and measured T_{pel} values. In figure 13, the simulated T_{pel} values at locations 2 and 3 are within 10% of the mean measured T_{pel} values. The simulated T_{pel} value at location 1 was underpredicted compared to the mean measured T_{pel} value. The sampling inlet at location 1 was in the fan jet zone, a region with a very high velocity gradient. This flow feature could lead to larger inaccuracies of simulations or of measurements at location 1. However, the simulated T_{pel} value at location 1 is still within 15% of the minimum measured T_{pel} value.

Table 11 lists the statistical evaluations for the CFD modeling protocol validation for the reception pit. The correlation coefficient of regression of simulated versus measured results (0.87) is 3% less than 0.9, the slope of regression is between 0.75 and 1.25 (0.88), and the intercept of regression (28.0) is slightly larger than 25% of the mean measured values (22.0).

DISCUSSION

The study results demonstrate that the CFD modeling protocols developed in this research satisfactorily predict the gas concentration decrease during forced ventilation in confined-space manure storages. The arguments supporting this assertion are:

For the solid cover case at the high and low AC rates, except for grid 1 (the sampling location closest to the fan jet), the difference between simulated and measured results is within 10% of the mean measured T_{pel} values at other sampling locations. However, at grid 1, the difference is still within 15% of the minimum measured T_{pel} value. Therefore, considering the complex flow feature in the vicinity of the fan area (high velocity gradient) and the effect of wind on inter-contamination strength, the CFD modeling protocols are considered adequate to predict H_2S concentration decrease in fan-ventilated confined-space manure storages with the solid cover.

For the partially slotted cover case at the high AC rate, the reason for unusual overprediction of simulated T_{pel} values of the upper level at grid 4 and grid 5 was caused primarily by differences in initial gas concentrations between tests. Ventilation times to reduce gas concentrations to 50% of initial concentrations (T_{50}) were used to normalize the effect of different initial concentration on simulated evacuation times at different sampling locations. Good agreement between simulated and measured T_{50} values demonstrates that the different initial concentration is the potential reason of unusual overprediction at grid 4 and grid 5 of the upper level at the high AC rate. In addition, the simulation inaccuracies of the CFD simulations arising from the complex flow feature in the vicinity of the fan area explained the underpredictions at grid 3 and grid 1 for the high and low AC rates, respectively. Based on these analyses, the CFD modeling protocols are considered adequate to simulate H_2S decay during forced ventilation in confined-space manure storages with the partially slotted cover.

For the fully slotted cover case at the high AC rate, grid 3 is the sampling location closest to the fan area (high velocity gradient). However, the simulated T_{pel} value at grid 3 is still within 15% of the minimum measured T_{pel} at the upper level and within 10% of the minimum measured T_{pel} at the lower level. The simulated T_{pel} values of grid 4 and grid 5 at the lower level are overpredicted compared to the measured values, however, they all are within 15% of the mean measured values. Therefore, considering the complex flow feature in the vicinity of the fan area and potential measurement errors, the CFD modeling protocols are considered adequate to predict H_2S evacuation from fan-ventilated confined-space manure storages with the fully slotted cover at the high AC rate.

For the fully slotted cover case at the low AC rate, the wind speed on the date of collecting concentrations decrease data was 24 km h^{-1}, which would tend to accelerate the removal of the gas from the slotted cover. However, the wind speed was not included as a boundary condition in the CFD simulations; therefore, the simulated values are for a wind speed of zero and thus would overpredict the measured values, especially at the upper level. In addition, the wind from the WSW direction blew the gas exhausted from the slots closest to location 1 of grid 4, which was located upwind of other sampling locations in one grid. Therefore, the wind with WSW direction most likely accelerated the gas removal, especially

at location 1 of grid 4 at the upper level. The simulations performed for the zero inter-contamination boundary condition and the measured inter-contamination boundary condition demonstrate the effect of high-velocity wind on the gas removal at the upper level of the tank. Considering the effect of wind speed and wind direction on gas removal from the manure tank, as well as the good agreement between simulated and measured T_{pel} values at locations 2 and 3 of grid 4 and grid 5, the CFD modeling protocols are deemed sufficient to predict H_2S concentration decrease during forced ventilation at the low AC rate.

For the independent manure reception pit, the simulated T_{pel} values of grid 2 and grid 3 are within 10% of the mean measured values. The simulated T_{pel} value at grid 4, a sampling location closest to fan area, is still within 15% of the minimum measured T_{pel} value. The good agreement between simulated and measured results shows that the CFD model satisfactorily simulated H_2S evacuation during forced ventilation in an independent on-farm manure reception pit. The data for determining the inter-contamination ratio and the gas concentration decrease data for validation for this facility were collected on the same date. The gas concentration decrease and inter-contamination data for the rectangular storage were collected on different dates. Consequently, there is higher degree of confidence in the magnitude of the inter-contamination boundary condition for this simulation than for the other simulations.

The statistical evaluations of the CFD model for the three cover cases and the independent manure reception pit show that the slope of regression is between 0.75 and 1.25 and the intercept of regression is less than 25% of the mean measured time for all the simulation cases. The correlation coefficients of regression do not satisfy the statistical criterion (>0.9) for all the simulation cases. However, except for the fully slotted cover case at the low AC rate (0.64), the correlation coefficients of other simulation cases are only slightly less than 0.9 (difference <8%). In addition, the correlation coefficient for the reception pit case, which has the best defined inter-contamination ratio, was 0.87, only 0.03 less than the ASTM D5157 target value of 0.9. Since the statistical criteria used (ASTM D 5157-97) were developed for highly controlled laboratory experimental systems, and since the respective statistics for our field study exceeded or nearly met the ASTM statistical criteria for successful CFD simulations, the CFD modeling protocols presented in this study appear to be satisfactory for simulating gas evacuation during forced ventilation of confined-space manure storages.

CONCLUSIONS

In this article, detailed validation procedures and results for three cover cases (i.e., solid, fully slotted, and partially slotted) are presented. The results obtained for these ventilation cases showed that the CFD modeling protocols were satisfactorily validated. The conclusions of this research are:

- The CFD code (PHOENICS 3.6) used in this research satisfactorily describes the flow feature of the jet flow and successfully simulates H_2S concentration decrease during forced ventilation in confined-space manure storage facilities.
- As an important boundary condition of the CFD simulations, the measured inter-contamination strength (ra-

tio of incoming contaminant concentration to contaminant concentration exhausted from outlet) needs to be adjusted when the wind velocity of the date for collecting the H_2S concentration decrease data is different from the date when the experiments were conducted for measuring inter-contamination strengths for three cover cases.

- The CFD modeling protocols (grid density evaluation, time step evaluation, outlet characterization, gas emission rate characterization, and inter-contamination characterization) were satisfactorily validated by the successful prediction of measured times to reach OSHA PEL for H_2S in the study confined-space rectangular manure tank for solid, fully slotted, and partially slotted cover cases for two air exchange rates (3 AC min^{-1} and 5 AC min^{-1}).

- The CFD modeling protocols (grid density evaluation, time step evaluation, outlet characterization, gas emission rate characterization, and inter-contamination characterization) were satisfactorily validated by the successful prediction of measured times to reach OSHA PEL for H_2S in an independent on-farm confined-space manure reception pit located at the Penn State Swine Center.

REFERENCES

ASTM. 2003. ASTM Standard D 5157-97: Standard guide for statistical evaluation of indoor air quality models. West Conshohocken, Pa.: American Society for Testing and Materials.

Beaver, R., and W. E. Field. 2006. Summary of documented fatalities in livestock manure storage and handling fatalities: 1975-2004. In *2006 Summer Conference of NIFS.* Paper No. 06-01. National Institute for Farm Safety.

CHAM. 2005. PHOENICS Version 3.6. London, U.K.: CHAM, Ltd.

CDC. 1993. Fatalities attributed to entering manure waste pits: Minnesota, 1992. *MMWR* 42(17): 325-329.

Chen, Q. 1995. Comparison of different k–ε models for indoor airflow computations. *Numerical Heat Transfer B* 28(3): 353-369.

Holmberg, S., and Q. Chen. 2003. Airflow and particle control with different ventilation systems in a classroom. *Indoor Air* 13(2): 200-204.

Lee, I., and T. Short. 2000. Two-dimensional numerical simulation of natural ventilation in a multi-span greenhouse. *Trans. ASAE* 43(3): 745-753.

Lloyd, W. E. 2000. Ventilation for confined space entry into underground manure storage facilities. MS thesis. University Park, Pa.: Pennsylvania State University, Department of Agricultural and Biological Engineering.

Millar, J. D. 1990. NIOSH Alert: Preventing deaths of farm workers in manure pits. Publication No. 90-103. Cincinnati, Ohio: NIOSH.

Murphy, D. J., and S. Steel. 2001. Manure storage hazards. Cooperative Extension Fact Sheet E28. University Park, Pa.: Pennsylvania State University.

OSHA. 1995. Air contaminants, 29 CFR 1910.1000. Washington, D.C.: OSHA.

OSHA. 1998. Permit-required confined spaces, OSHA 3138. Washington, D.C.: OSHA.

OSHA. 2002. Application of the permit-required confined spaces (PRCS), 29 CFR 1910.146. Washington, D.C.: OSHA.

Pesce, E. 2005. Screening ventilation strategies for confined space manure storages. Unpublished MS thesis. University Park, Pa.: Pennsylvania State University, Department of Agricultural and Biological Engineering.

Pesce, E, J. Zhao, H. B. Manbeck, and D. J. Murphy. 2007. Screening ventilation strategies for confined-space manure storages. *J. Agric. Safety and Health* (in review).

Sørensen, D. N., and P. V. Nielsen. 2003. Quality control of computational fluid dynamics in indoor environments. *Indoor Air* 13(1): 2-17.

Srebric, J., and Q. Chen. 2002. An example of verification, validation, and reporting of indoor environment CFD analysis. *ASHRAE Trans.* 108(2): 185-194.

Sun, H., L. Zhao, and Y. Zhang. 2007. Evaluation of RNG κ–ε and LES non-isothermal models for indoor airflow using PIV measurement data. *Trans. ASABE* 50(2): 621-631.

Versteeg, H. K., and W. Malalasekera. 1995. *An Introduction to Computational Fluid Dynamics.* Upper Saddle River, N.J.: Addison-Wesley.

Zhao, J. 2006. Simulation and validation of hydrogen sulfide removal from fan-ventilated confined-space manure storages. PhD diss. University Park, Pa.: Pennsylvania State University, Department of Agricultural and Biological Engineering.

Zhao, J., H. B. Manbeck, and D. J. Murphy. 2007. H_2S emission rates and inter-contamination measurements in fan-ventilated confined-space manure storages. *Trans. ASABE* 50(6): (in press).